Available online at www.sciencedirect.com
ScienceDirect
Trans. Nonferrous Met. Soc. China 30(2020) 344−362
Transactions of Nonferrous Metals Society of China
www.tnmsc.cn

Effect of laser surface melting on surface integrity of Al−4.5Cu composites reinforced with SiC and MoS_2

Praveen Kumar BANNARAVURI[1], Anil Kumar BIRRU[2], Uday Shanker DIXIT[3]

1. Department of Mechanical Engineering, Karunya Institute of Technology and Science, Coimbatore, Tamil Nadu 641114, India;
2. Department of Mechanical Engineering, National Institute of Technology Manipur, Imphal 795004, India;
3. Department of Mechanical Engineering, Indian Institute of Technology Guwahati, Assam 781039, India

Received 23 April 2019; accepted 27 December 2019

Abstract: Two types of composites were prepared with Al−4.5Cu alloy as a matrix using stir casting method. One was reinforced with 10 wt.% of SiC and 2 wt.% of MoS_2. The other was reinforced with 10 wt.% of SiC and 4 wt.% of MoS_2. Their surfaces were remelted using a CO_2 laser beam with an objective to study the influence of laser surface melting (LSM). The topography, microhardness, corrosion resistance and wear resistance of the laser melted surfaces were studied. Overall surface integrity after LSM was compared with as-cast surface. LSM enhanced the microhardness and wear resistance of the surface in each case. Porosity of the laser melted surface was low and corrosion resistance was high. Thus, LSM can be conveniently applied to enhancing the surface integrity of the aluminium composites. However, there is an optimum laser specific energy, around 38 J/m^2 in this study, for obtaining the best surface integrity.
Key words: aluminium composites; silicon carbide; molybdenum disulfide; laser surface melting; microhardness; corrosion resistance

1 Introduction

Aluminum alloys have gained rapid popularity in the last few decades, especially in automobile and aerospace industries due to their easy availability, low density, high specific strength, and easy processing [1]. However, these alloys often exhibit inadequate surface properties such as wear and corrosion resistances, leading to their frequent replacement [2]. The ceramic particle reinforced composites of aluminium alloy provide good corrosion and wear resistances [3,4]. In addition, aluminium composites have good hardness, high specific strength and good chemical stability [5−8], making them suitable for use in machine parts. A number of researchers studied the mechanical properties of aluminum composites.

SINGH and GOYAL [9] noted that mechanical properties were enhanced with the addition of SiC and B_4C in the Al6082-T6 matrix alloy by stir casting method. The agglomeration of particles can be observed in the hybrid composites with the increase in amount of reinforcement particles. SINGH et al [10] reported that in the Al-6063 matrix alloy, the addition of large grain SiC and Al_2O_3 particles resulted in high porosity; reducing the grain size reduced the porosity. The addition of fine reinforcing particles improved the strength drastically. Reinforcing particles need to be homogeneously distributed in the bulk composite material to attain good mechanical and tribological properties [11]. Nonhomogeneous surface of the composites is prone to many surface defects like pores, voids, segregation and agglomeration of the particles [12]. Hence, some processes are needed to

Corresponding author: Uday Shanker DIXIT; E-mail: uday@iitg.ac.in
DOI: 10.1016/S1003-6326(20)65217-7

improve the surface properties of composite material [13,14].

In the recent years, laser has been used to improve surface properties by laser surface melting (LSM) [15], alloying [16] and cladding [17]. LSM is a well-established process for hardening, minimizing porosity as well as increasing wear and corrosion resistances of surface. LSM is a versatile and promising technique thanks to its ability to modify the surface properties of a material without affecting the bulk property [18,19]. LSM provides precision of operation, fast processing time, and local treatment. The modification of the surface properties of the material is due to rapid melting followed by rapid solidification. The high cooling rate is the characteristic of LSM that results in a significantly refined microstructure. Redistribution of precipitates leads to the improved surface properties [20,21].

The laser surface treatment of aluminium alloys has been widely investigated since last decade [22,23]. LSM was applied to aluminium composites but the available literature is sparse. WONG and LIANG [24] reported that after LSM of Al−Si alloys (0−13 wt.% Si) using continuous wave (CW) CO_2 laser machine, the solubility of Si was enhanced beyond its equilibrium saturation limit. The corrosion rates of the Al−Si alloys in 10% H_2SO_4 and 10% HNO_3 solutions were less, but the corrosion rates in chloride solution containing 10% HCl and 5% NaCl did not reduce after LSM. The microstructure refinement on the surface of Al−9%Si aluminium alloy by LSM with 1 kW CW CO_2 laser machine was accomplished with reduction in the dendritic arm spacing to one-fifth that of the as-cast alloy [25]. HU et al [26] fabricated Al2024/$Al_{18}B_4O_{33w}$ composite containing 20% (volume fraction) of whisker by squeeze casting method. LSM was performed under N_2 atmosphere by the Nd:YAG pulse laser having a wavelength of 1064 nm. On the surface of the composite, γ-Al_2O_3 appeared due to the decomposition of whiskers after LSM. The microhardness was improved due to fine dendritic microstructure and solid solution hardening.

LSM process helps in proper bonding of hard ceramic particles and aluminium matrix alloy, enhancing the corrosion and wear resistances. However, high stress levels may cause asperities such as micro-cracks [27]. YILBAS et al [28] carried out LSM on the surface of hot-pressed aluminum matrix alloy reinforced with 15 wt.% of B_4C particles. It was noticed that there were no micro-cracks or pores on the laser-treated surface due to self-annealing effect. Grain refinement with uniform distribution of B_4C particles was observed, resulting in increased hardness of the laser-treated surface. The laser-treated surface also has low roughness and coefficient of friction. Till now, the surface modification of aluminium hybrid composites Al−4.5Cu/SiC/MoS_2 by LSM has not been studied.

In this work, LSM of aluminum Al−4.5Cu alloy and its composites with SiC and MoS_2 particles was carried out. One composite contained 10 wt.% SiC and 2 wt.% MoS_2. The other composite contained 10 wt.% SiC and 4 wt.% MoS_2. The experiments were carried out by varying laser specific energy (LSE). After LSM, the surface integrity was studied and compared with that of the as-cast material. A definite improvement was observed due to LSM.

2 Experimental

2.1 Fabrication of composite material by stir casting method

The aluminium alloy Al−4.5Cu (wt.%) was selected as the matrix material. The chemical composition of the studied alloy by a optical emission spectrometer (ICP−OES) is shown in Table 1. Among various discontinuous (particle) reinforcements available for the synthesis of aluminium composites, SiC (average particle size of 35 μm and density of 3.21 g/cm^3) and MoS_2 (average particles size of 35 μm and density of 5.06 g/cm^3) were selected as reinforcements to enhance the strength of the composite. Magnesium in ingot form was used to improve the wettability between the matrix alloy and reinforcements during the production of the composite materials [29].

Table 1 Chemical composition of Al−4.5Cu alloy (wt.%)

Cu	Mg	Si	Fe	Mn	Ni
4.52	0.066	0.538	0.663	0.131	0.075
Pb	Sn	Ti	Zn	Al	
0.029	0.021	0.013	0.118	Bal.	

Figure 1 illustrates a flowchart of method for aluminium composites fabrication by stir casting method. The two types of composite ingots were fabricated, Al−4.5Cu/10SiC/2MoS_2 and Al−4.5Cu/10SiC/4MoS_2, where numerals indicate mass fraction.

2.2 LSM of composite fabricated by 2.5 kW CO_2 laser machine

Stir cast samples were sectioned to rectangular blocks with dimensions 20 mm × 10 mm × 10 mm for surface melting by laser. The surfaces of the specimens were melted by using a CO_2 laser machine (Model: Orion 3015, Make: LVD, Belgium) shown in Fig. 2(a) at a wavelength of 10.6 μm. The power of laser machine can be varied in the range of 100−2500 W. A schematic diagram of LSM is shown in Fig. 2(b).

The absorptivity of aluminium composite was improved by coating the sample with graphite prior to melting [30,31]. The laser power (P) was varied from 1.8 to 2.0 kW, the laser beam diameter (d) range was 4.72–6.07 mm, standoff distance (H) range was 35–45 mm and a constant scan speed (v) of 400 mm/s was maintained. Argon shielding gas was used during the laser melting process to prevent oxidation. Table 2 shows laser parameters used for surface re-melting of Al−4.5Cu composites.

The laser beam diameter (d) was calculated as follows [32]:

$$d = 2w_0\left[1+\left(\frac{M^2\lambda H}{\pi w_0^2}\right)^2\right]^{1/2} \quad (1)$$

where w_0=0.05 mm is the laser beam waist, which is the minimum beam diameter at the focal point of the lens, λ=10.6 μm is the CO_2 laser beam wavelength, and M^2 is the beam quality factor, taken as 1.4 based on KANT et al [33]. An important parameter is the laser specific energy E that can be calculated as [34]

$$E = \frac{P}{vd} \quad (2)$$

2.3 Microstructure and XRD analysis

The metallographic examination of the as-cast and LSM-treated samples was carried out using optical microscopy (OM) and scanning electron microscopy (SEM) with energy dispersive X-ray spectroscopy (EDX). For the examination of the microstructure, the composite samples were sectioned into 10 mm × 5 mm × 10 mm blocks. Different grades of silicon carbide grit sheets were used starting from rough to fine grades, viz, 120, 240, 360, 600, 800, 1200, 1500 and 2000 grit size.

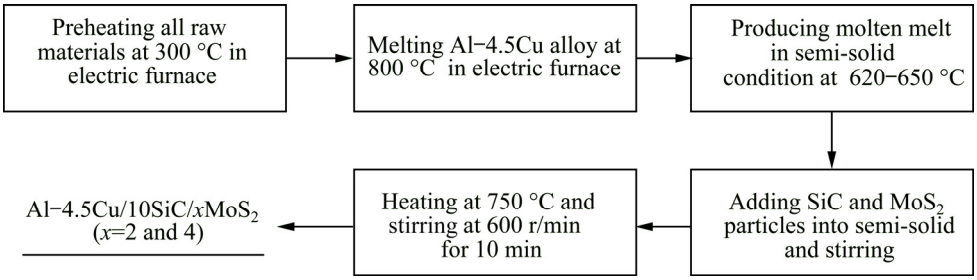

Fig. 1 Flowchart of fabrication of aluminium composites by stir casting method

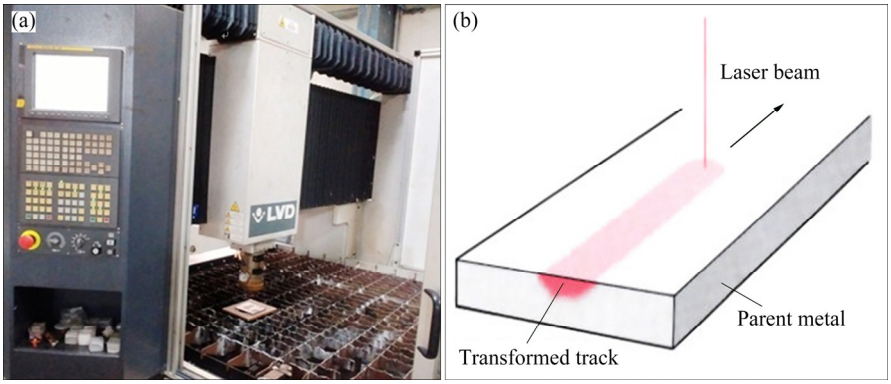

Fig. 2 Experimental setup (a) and schematic diagram (b) of laser surface melting

Table 2 Laser parameters used for surface re-melting of composites

Sr. No.	Material	Laser parameter			
		P/ kW	*H*/ mm	*d*/ mm	*E*/ (J·mm^{-2})
1	Al−4.5Cu	1.8	35	6.61	41
2	Al−4.5Cu	1.8	40	7.56	36
3	Al−4.5Cu	1.8	45	8.5	32
4	Al−4.5Cu	1.9	35	6.61	43
5	Al−4.5Cu	1.9	40	7.56	38
6	Al−4.5Cu	1.9	45	8.5	34
7	Al−4.5Cu	2.0	35	6.61	45
8	Al−4.5Cu	2.0	40	7.56	40
9	Al−4.5Cu	2.0	45	8.5	35
10	Al−4.5Cu/10SiC/2MoS_2	1.8	35	6.61	41
11	Al−4.5Cu/10SiC/2MoS_2	1.8	40	7.56	36
12	Al−4.5Cu/10SiC/2MoS_2	1.8	45	8.5	32
13	Al−4.5Cu/10SiC/2MoS_2	1.9	35	6.61	43
14	Al−4.5Cu/10SiC/2MoS_2	1.9	40	7.56	38
15	Al−4.5Cu/10SiC/2MoS_2	1.9	45	8.5	34
16	Al−4.5Cu/10SiC/2MoS_2	2.0	35	6.61	45
17	Al−4.5Cu/10SiC/2MoS_2	2.0	40	7.56	40
18	Al−4.5Cu/10SiC/2MoS_2	2.0	45	8.5	35
19	Al−4.5Cu/10SiC/4MoS_2	1.8	35	6.61	41
20	Al−4.5Cu/10SiC/4MoS_2	1.8	40	7.56	36
21	Al−4.5Cu/10SiC/4MoS_2	1.8	45	8.5	32
22	Al−4.5Cu/10SiC/4MoS_2	1.9	35	6.61	43
23	Al−4.5Cu/10SiC/4MoS_2	1.9	40	7.56	38
24	Al−4.5Cu/10SiC/4MoS_2	1.9	45	8.5	34
25	Al−4.5Cu/10SiC/4MoS_2	2.0	35	6.61	45
26	Al−4.5Cu/10SiC/4MoS_2	2.0	40	7.56	40
27	Al−4.5Cu/10SiC/4MoS_2	2.0	45	8.5	35

The final mirror polishing was done using a velvet cloth by applying chemical Silvo. After drying samples, etching was done using standard Keller's reagent comprising 2 mL HF, 3 mL HCl, 5 mL HNO_3, and 190 mL distilled water. The XRD pattern of the LSM composites was obtained with filtered Cu $K_{\alpha 1}$ radiation (λ=0.154056 Å) at a voltage of 40 kV and current of 20 mA.

2.4 Density and surface microhardness measurement

The experimental density for each composite was evaluated by weighing the test sample using a high precision electronic weighing balance with a tolerance of 0.1 mg. The measured mass in each case was divided by the volume of the respective sample. The experimental density of composites was determined by water displacement technique (Archimedes' principle) and is calculated as follows [35]:

$$\rho_{ex} = \frac{m}{V} \tag{3}$$

where ρ_{ex} is the experimental density of specimen, m is the mass of the specimen and V is the volume of water displaced.

The surface microhardness of as-cast and LSM-treated composites was measured. Hardness tests were carried out by taking the average of three readings for each sample using a Vickers hardness tester. A diamond indenter tip was pressed on the surface of the sample to make indentation mark at a load of 0.98 N. The hardness of the sample was calculated by measuring the dimension of indentation mark observed on the surface with a dwelling time of 15 s.

2.5 Corrosion measurement

Corrosion immersion test was conducted for as-cast and LSM-treated composites. Samples were sectioned in the form of blocks with dimensions of 10 mm × 5 mm × 10 mm. Then, the samples were mounted with phenol resin that resisted corrosion due to salt and acidic solutions. The portion of the surface to be tested for corrosion was exposed to corrosive media (NaCl and H_2SO_4) for 200 h. The pH of the solution was measured before corrosion test by pH meter. After corrosion test, samples were cleaned using acetone and dried. The mass of samples before and after corrosion test was measured by using a precise electric mass measuring machine with an accuracy of 0.1 mg. The mass loss was measured to assess damage on surface of as-cast and LSM-treated composites and corrosion damage was analyzed by SEM.

2.6 Dry sliding wear test

Wear resistance of LSM-treated materials (at LSE of 38 J/mm^2) was investigated with pin-on-disc wear test machine and the values were compared with those of as-cast materials. The rotating counter disk was made of EN-32 steel of hardness HRC 65. The pin was cylindrical with

10 mm in diameter and track diameter was 80 mm. Wear test parameters were taken as applied loads of 10 and 30 N, sliding speeds of 1.5 and 3.5 m/s and a constant sliding distance of 2000 m. The test pin mass was measured by a digital electronic balance with an accuracy count of 0.1 mg before and after the wear test. If m_1 is the initial mass of the material and m_2 is the mass after wear of the material, the volume loss V_l is given by

$$V_l = \frac{m_1 - m_2}{\rho} \tag{4}$$

where ρ is the density of the test pin. The wear rate W_r is given by

$$W_r = \frac{V_l}{D} \tag{5}$$

where D is the sliding distance. The wear mechanism was studied by observing the worn surface morphology of aluminium composites with the scanning electron microscopy (SEM).

3 Results and discussion

The microstructures of as-cast and LSM-treated samples were analyzed by optical and electron microscopy.

3.1 Microstructures

The microstructures of the as-cast matrix and composites are depicted in Fig. 3. The microstructure of the as-cast Al−4.5Cu alloy comprises large primary α(Al) dendrites, eutectic copper between dendrite arms and intermetallic compounds ($CuAl_2$) appearing as particles along the dendrite boundaries (Fig. 3(a)). Microstructures of the as-cast composites, Al−4.5Cu/10SiC/2MoS_2 and Al−4.5Cu/10SiC/4MoS_2 were analyzed through optical micrographs in order to find out the distribution of reinforcement particles in matrix material (Figs. 3(b) and (c)). It is seen that the reinforcement particles are reasonably uniformly distributed in the matrix. Uniform distribution of reinforcement particles may be attained by increasing wettability between matrix and reinforcement. Hence, the matrix melt was stirred by impeller and magnesium was added in the melt as suggested in Ref. [29].

According to GUI et al [36], microstructural refinement in the composites occurs due to the presence of reinforcement particles, which may act as sites of nucleation in the solidification process of the melt. Grain size refinement can be considerable with the presence of ceramic particles. Porosity and micro-segregations are common defects that may favour the localized corrosion process [37]. Here, at some places, particle agglomeration can occur with

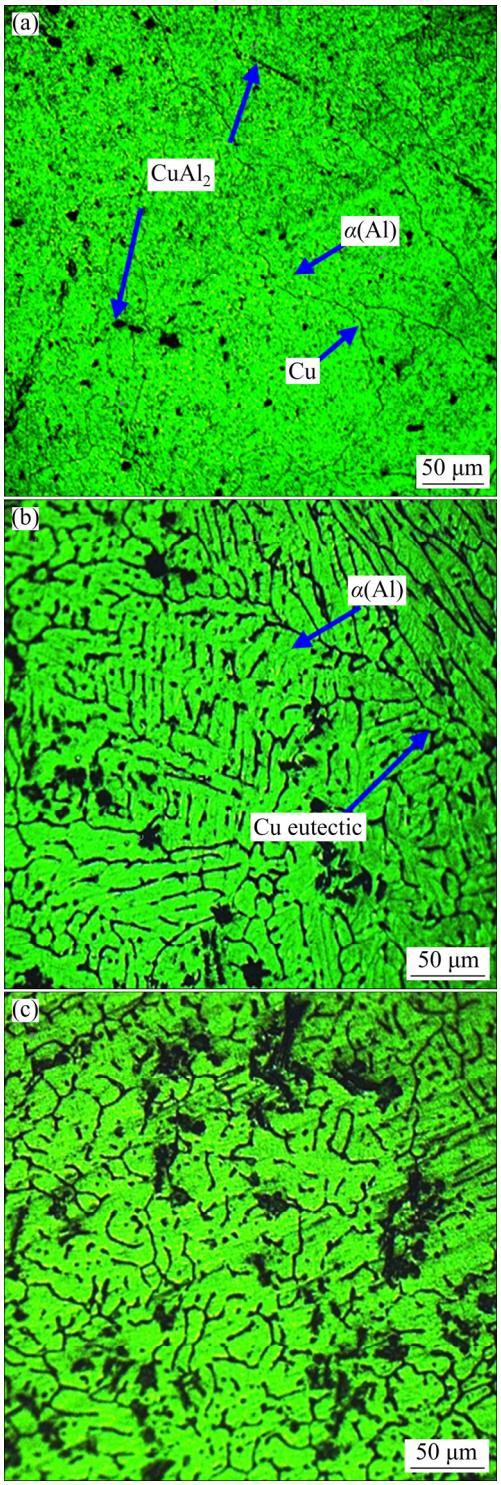

Fig. 3 Microstructures of as-cast Al−4.5Cu alloy (a), Al−4.5Cu/10SiC/2MoS_2 (b) and Al−4.5Cu/10SiC/4MoS_2 (c)

voids at interdendritic spaces in the composites as apparent from Fig. 4.

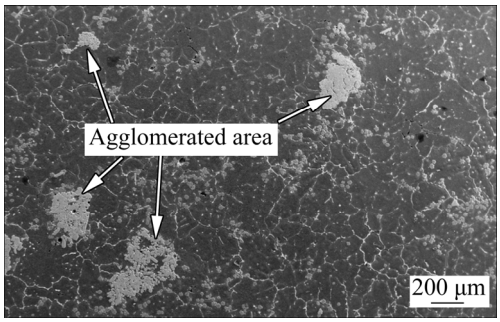

Fig. 4 SEM micrograph of as-cast Al−4.5Cu/10SiC/4MoS_2 composites showing agglomeration

The porosity was observed in the matrix due to entrapped gases in the molten metal during solidification as shown in Fig. 3(a). Figures 3 and 4 show the noticeable amount of blow holes or pin holes caused due to contact with ambient gases during the stirring process [38]. The volume of the porosity, characterized by the size and distribution of pin/blow holes, plays a vital role in altering the mechanical properties of the composites. The load-bearing capacity of material is reduced due to porosity as it also causes stress concentration. Blow/pin holes in surface and near-surface regions strongly reduce high cycle fatigue strength [39]. It is crucial to eliminate these defects mainly on the surface. Hence, several researchers investigated LSM for modifying the surface [40]. The microstructures of the LSM-treated matrix and composites at various LSEs are shown in Figs. 5−12. These microstructures are obtained after polishing the samples, in which 50−100 μm thick layers of material are removed from the surface; LSM produces a surface with 8−10 μm centreline average surface roughness. The melting starts from top of the surface and penetrates towards substrate portion when laser beam scans the surface of material. The solidification starts from the interface between LSM region and substrate. The hardening rate of the surface of material may depend on cooling rate at liquid−solid boundary, the increase in the solid solubility and concentrations of alloying elements [22]. The microstructures of LSM matrix are shown in Fig. 5 at LSEs of 32, 38 and 45 J/mm^2, respectively. In the LSM process, the solidification rate is very high. As a result of the rapid solidification of the laser-melted zone, finer grains

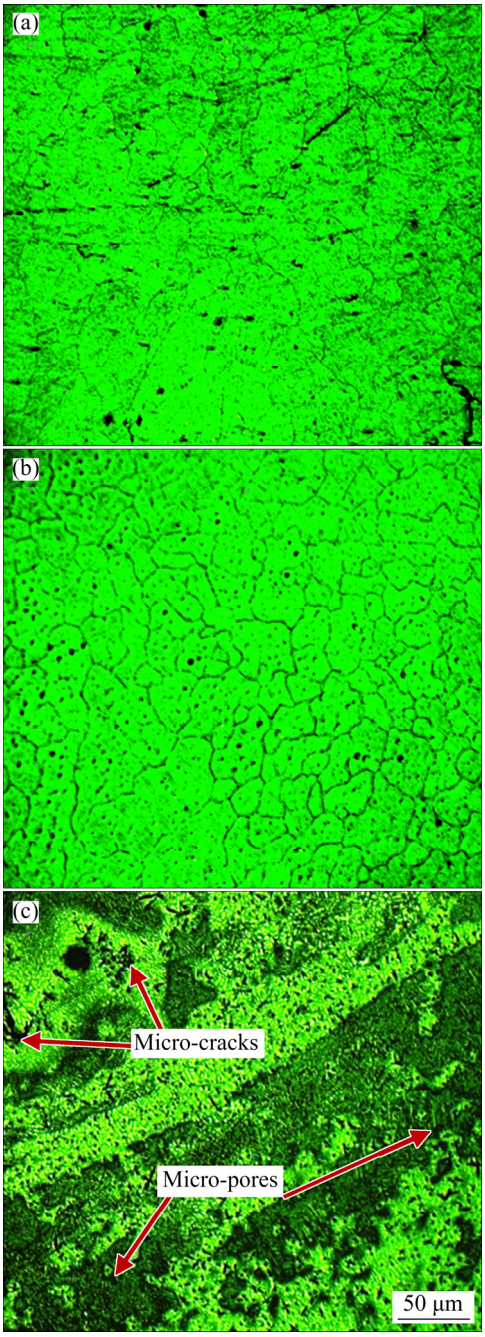

Fig. 5 Microstructures of LSM-treated Al−4.5Cu matrix alloy at various LSEs: (a) 32 J/mm^2; (b) 38 J/mm^2; (c) 45 J/mm^2

are formed compared to the untreated zone as shown in Fig. 6. LSM refines the microstructural features [41]; it forms dendritic grains and minimizes inter-dendrite spacing.

The solidification rate of the molten pool mainly depends on the LSE and the interaction period of the laser beam with material [42]. The depth of melting also depends on LSE. At a lower LSE of 32 J/mm^2, no obvious structural changes are

observed as shown in Fig. 5(a) due to insufficient melting. The fine grain refinement of matrix without defects is observed at LSE of 38 J/mm^2 as shown in Fig. 5(b) in comparison with as-cast matrix (Fig. 3(a)). In this case, the porosity of surface of matrix alloy is not found after LSM due to appropriate melting and solidification. At high LSE of 45 J/mm^2, many micro-porosities and micro-cracks are observed in the optical image shown in Fig. 5(c) and SEM image shown in Fig. 7. SEM micrograph of matrix (Fig. 7(a)) shows intermetallic compounds such as $CuAl_2$ in the alloy zone. The results at higher LSE show the formation of cracks (Fig. 7(b)) due to reduced ductility of the surface of material.

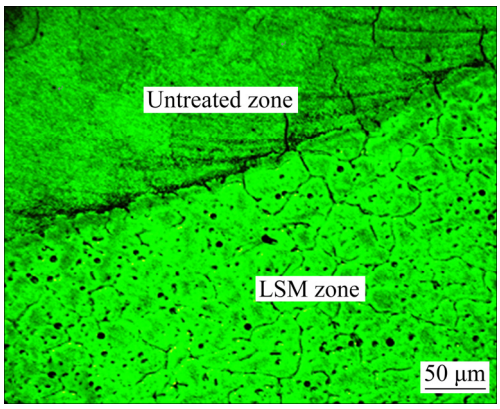

Fig. 6 Microstructure of laser-treated at LSE of 38 J/mm^2 (bottom) and untreated zone (top) of matrix alloy

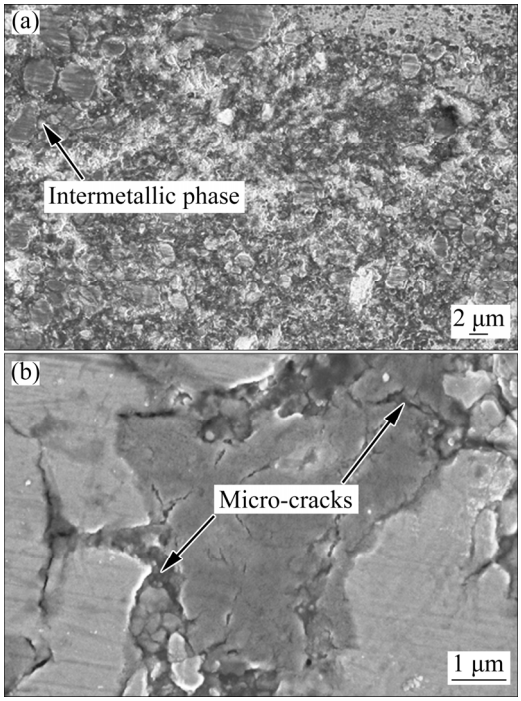

Fig. 7 SEM images of LSM-treated Al−4.5Cu alloy at LSE of 45 J/mm^2: (a) Intermetallic phase; (b) Micro-cracks

The microstructures of Al−4.5Cu/10SiC/2MoS_2 composite after LSM are shown in Fig. 8, at LSEs of 32, 38 and 45 J/mm^2, respectively. At lower LSE of 32 J/mm^2, there is no significant change in microstructure as shown in Fig. 8(a) in comparison with as-cast material (Fig. 3(b)). The noticeable grain refinement of composite is observed at LSE of 38 J/mm^2 as shown in Fig. 8(b).

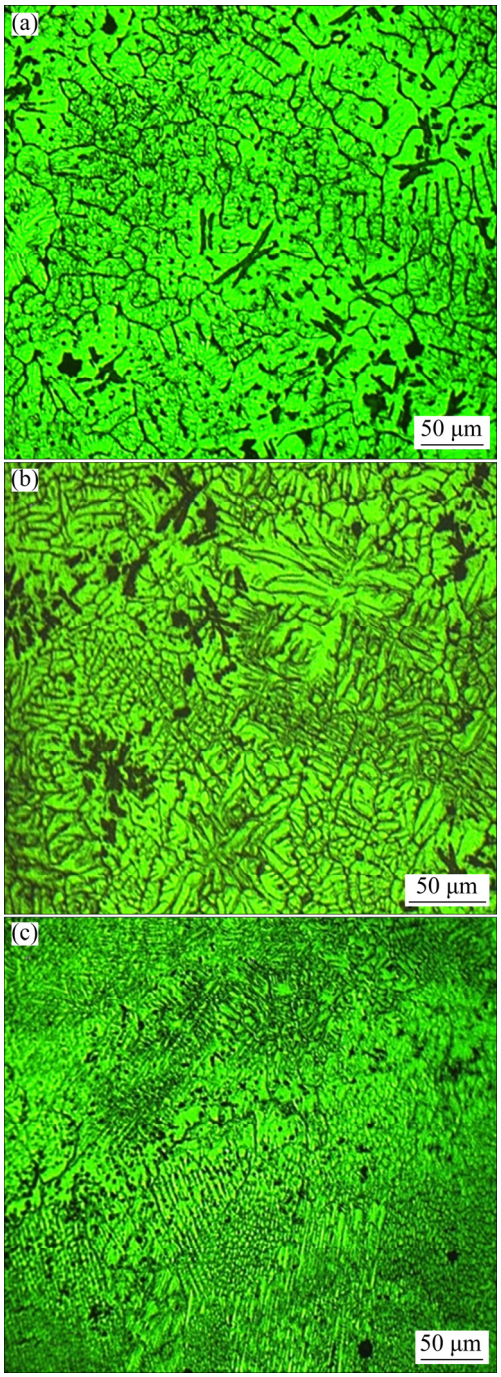

Fig. 8 Microstructures of LSM-treated Al−4.5Cu/10SiC/2MoS_2 composite at various LSEs: (a) 32 J/mm^2; (b) 38 J/mm^2; (c) 45 J/mm^2

In addition, at LSE of 45 J/mm^2, micro-cracks and coarser grains are observed as shown in Fig. 8(c). The microstructures of Al−4.5Cu/10SiC/4MoS_2 composites after LSM are shown in Fig. 9. At lower LSE of 32 J/mm^2, the same trend is noticed as shown in Fig. 9(a) as observed in the case of Al−4.5Cu/10SiC/2MoS_2 composite. At LSE of 38 J/mm^2, the grain size of the Al−4.5Cu/10SiC/4MoS_2 composites is reduced, as shown in Fig. 9(b). However, no micro-cracks are observed around the hard particles after the rapid solidification of the surface. Melting depth mainly depends on the LSE, which also affects cooling rate and time. A higher LSE of 45 J/mm^2 creates wider and deeper remelted layer thickness than LSE of 38 J/mm^2, as shown in Fig. 10. The depth of melting is about 330 μm at LSE of 38 J/mm^2, as shown in Fig. 10(a) and approximately 516 μm at 45 J/mm^2, as shown in Fig. 10(b). The increase in cooling time results in the formation of coarser grains in the composites, as shown in Fig. 9(c).

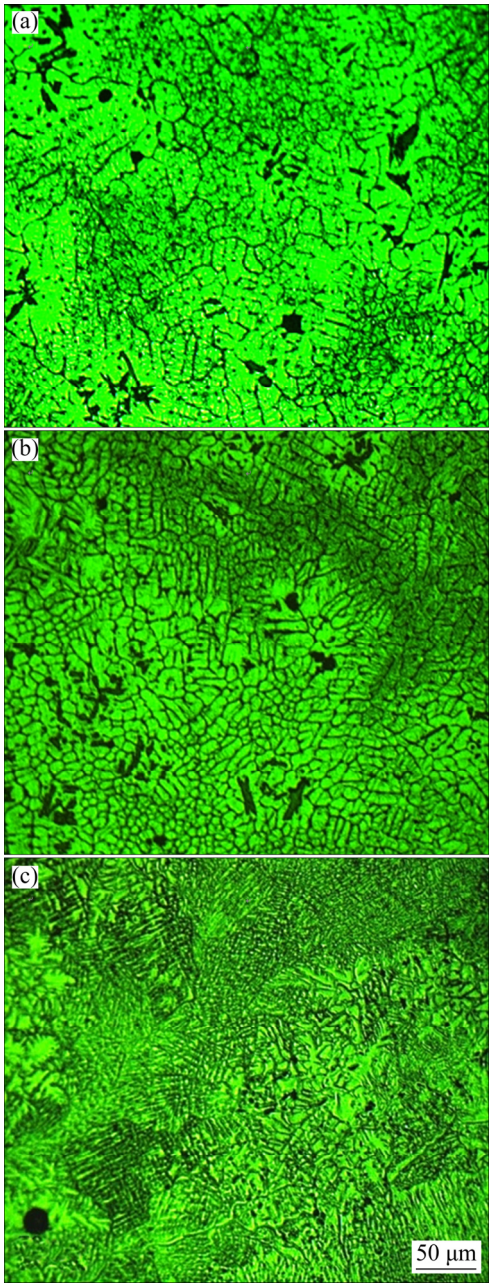

Fig. 9 Microstructures of LSM-treated Al−4.5Cu/10SiC/4MoS_2 composite at various LSEs: (a) 32 J/mm^2; (b) 38 J/mm^2; (c) 45 J/mm^2

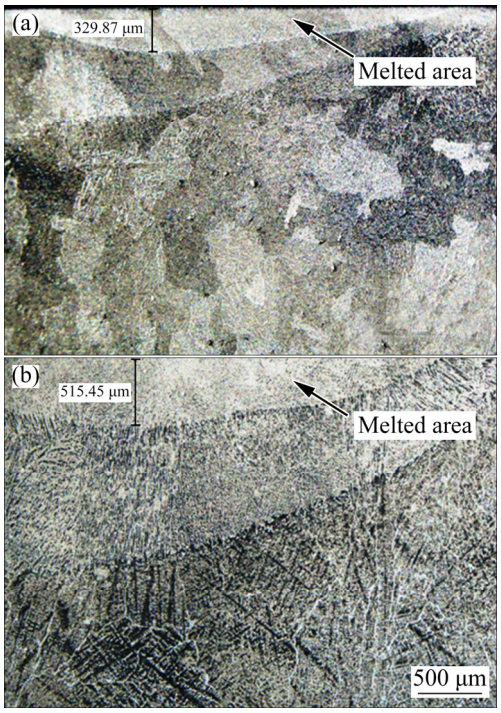

Fig. 10 Cross-section views of Al−4.5Cu/10SiC/4MoS_2 composites after LSM at various LSEs: (a) 38 J/mm^2; (b) 45 J/mm^2

The surface of composite melted by laser beam may create new phase transformation that refines the microstructure and avoids the particle agglomeration by forming a homogeneous distribution of particles. In the LSM process of Al−4.5Cu/10SiC/4MoS_2 composite at LSE of 38 J/mm^2, the reinforcement particles are uniformly distributed in the matrix, as shown in Fig. 11(a). Strong bonding with clear interface is observed between matrix and reinforcement particles, as shown in Fig. 11(b). For a higher LSE of 45 J/mm^2, a typical microstructure of Al−4.5Cu/10SiC/4MoS_2 composite is shown in Fig. 12, which reveals the agglomeration (Fig. 12(a)) of ceramic particles. Eventually cracked ceramic particles are observed, as shown in Fig. 12(b); the figure also shows micro-pores and micro-crevices close to the reinforcement particles, especially near agglomerated particles.

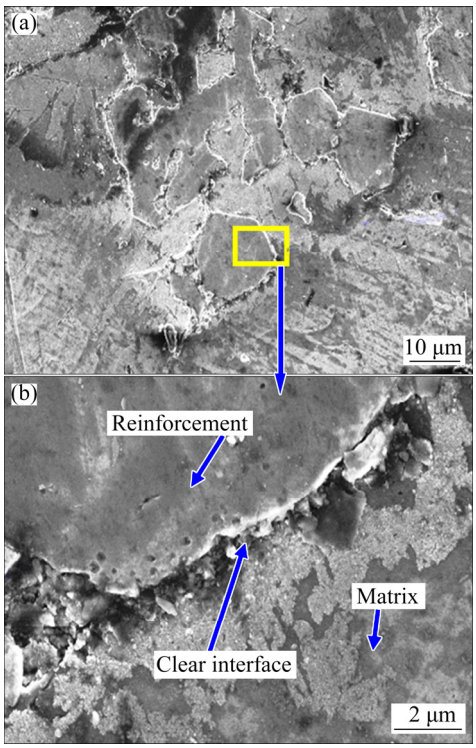

Fig. 11 SEM images of LSM-treated Al−4.5Cu/10SiC/4MoS_2 composite at LSE of 38 J/mm^2 showing uniform distribution of particles (a) and clear interface between matrix and reinforcement (b)

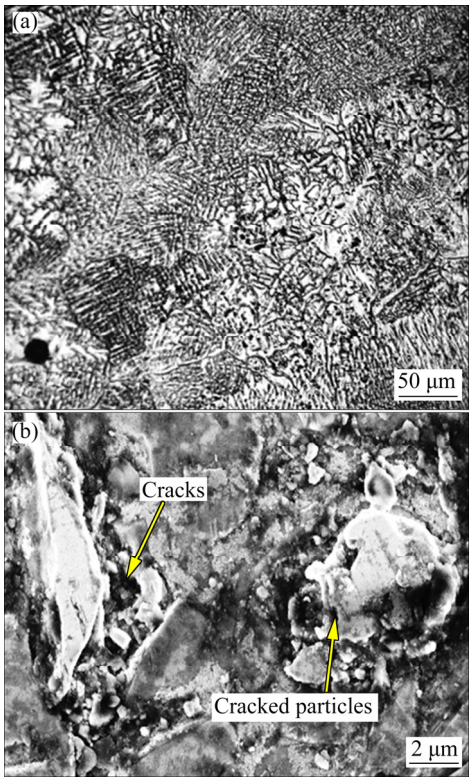

Fig. 12 Microstructures of Al−4.5Cu/10SiC/4MoS_2 composite after LSM at LSE of 45 J/mm^2: (a) Optical image showing agglomeration; (b) SEM image showing cracks

The average grain size of samples was calculated using mean linear intercept method. Figure 13 shows the average grain size of the as-cast and LSM-treated (at LSE of 38 J/mm^2) matrix and composite materials. Noticeable reduction in average grain size of material after LSM is observed in comparison with as-cast material due to rapid solidification after LSM. A rapid solidification induced by laser (at LSE of 38 J/mm^2) without any deliberate change in chemical composition of surface of LSM-treated hybrid composite is confirmed from EDX mapping images, as shown in Fig. 14. EDX mapping images for as-cast hybrid composite Al−4.5Cu/10SiC/4MoS_2 are shown in Fig. 15. The results indicate the surface modification after LSM. Similarly, SUREKHA et al [43] studied the structural modification of AA2219-T87 alloy by LSM using 4 kW CO_2 laser machine and observed the grain refinement of material due to high cooling rate.

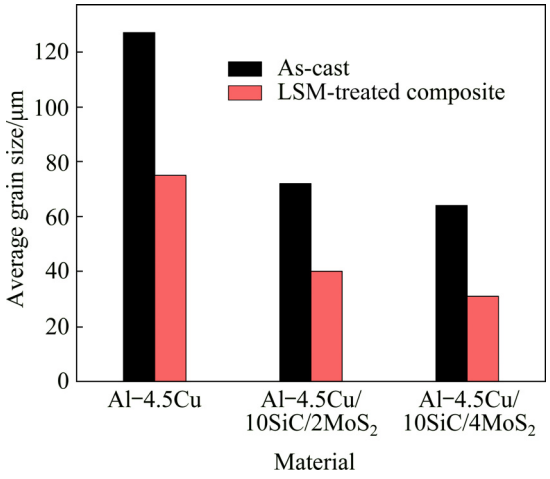

Fig. 13 Average grain size of as-cast and LSM-treated composite material at LSE of 38 J/mm^2

3.2 XRD patterns

The XRD patterns of LSM-treated matrix alloy and hybrid composites at LSE of 38 J/mm^2 are shown in Fig. 16. Figure 16 shows the presence of Al and Cu elements and formation of intermetallic phase or reaction layers such as $CuAl_2$ in melted surface of matrix; it confirms SEM images shown in Fig. 7. It is clear from Fig. 16 that the aluminium peaks in the LSM-treated composites are fairly shifted to lower 2θ in comparison to matrix alloy. The shifting of aluminium peaks may occur due to the presence of reinforcement particles in the composite materials. Thermodynamically, SiC and

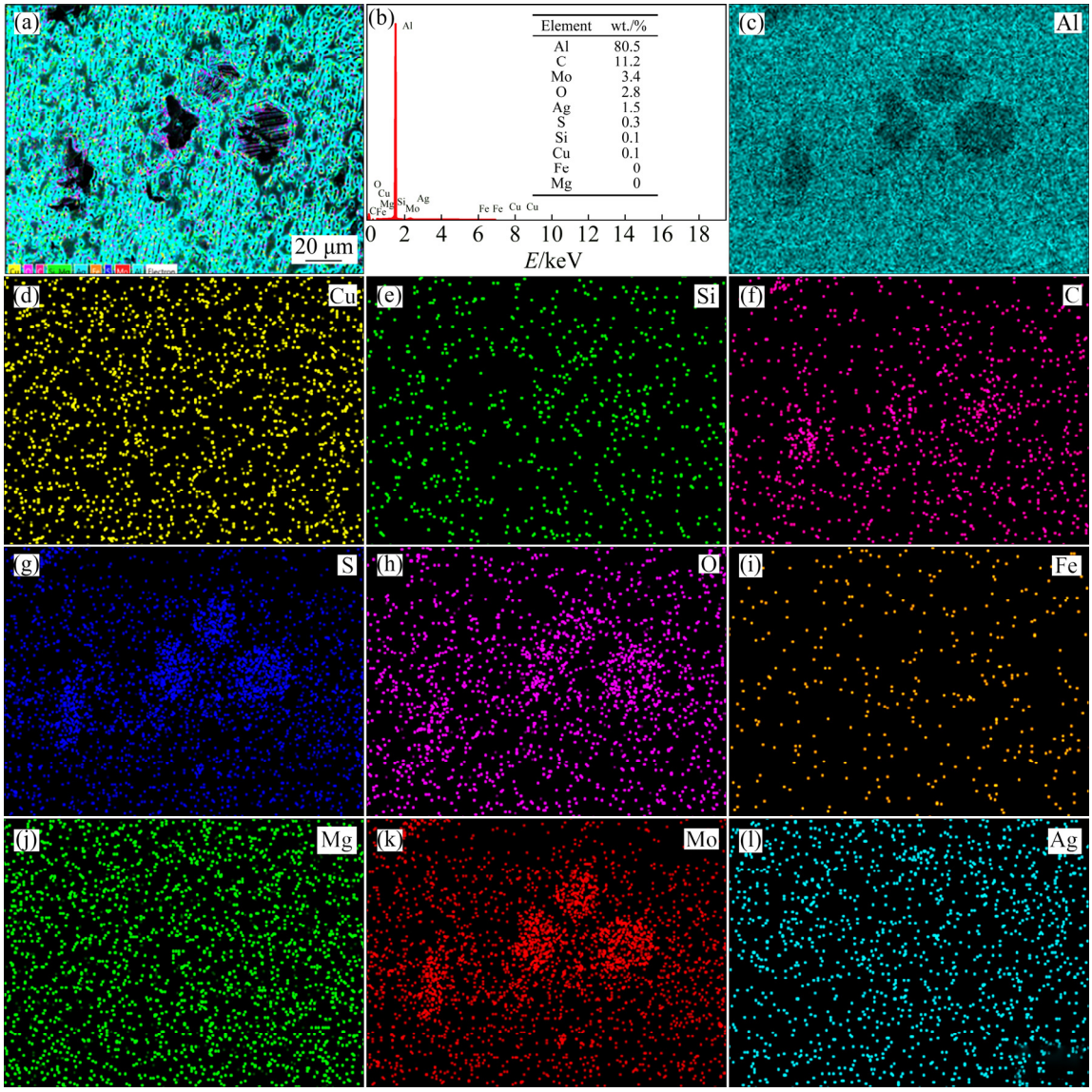

Fig. 14 SEM image (a), EDS spectrum (b) and element mapping images (c−l) of LSM-treated Al−4.5Cu/10SiC/4MoS_2 composite at LSE of 38 J/mm^2

MoS_2 particles remain inert in the LSM process condition. Ceramic particles may not decompose and interact with the matrix to generate any kind of intermetallic elements.

3.3 Experimental density and microhardness

The experimental density and microhardness values of as-cast matrix and composites were measured and compared. Figure 17 shows the microhardness and experimental density of as-cast matrix and composites. The density of the composite increases with an increase in reinforcement due to higher density of reinforced SiC and MoS_2 as shown in Fig. 17(a). The average microhardness values of as-cast matrix and composites were observed to be $HV_{0.1}$ 84, $HV_{0.1}$ 116 and $HV_{0.1}$121, as shown in Fig. 17(b). The microhardness increases with the addition of secondary-phase reinforcement (SiC and MoS_2) in the composite. Reinforcing the matrix with 10 wt.% of SiC and 2 wt.% of MoS_2 increases the microhardness by about 50%. On the other hand, there is no significant difference in the microhardness for Al−4.5Cu/10SiC/2MoS_2 and Al−4.5Cu/10SiC/4MoS_2; 2 wt.% increase in MoS_2 increases the average microhardness only slightly. This is because SiC is much harder than MoS_2.

The microhardness values of LSM-treated matrix and composites are depicted in Fig. 18 at various LSEs. LSM enhances the microhardness

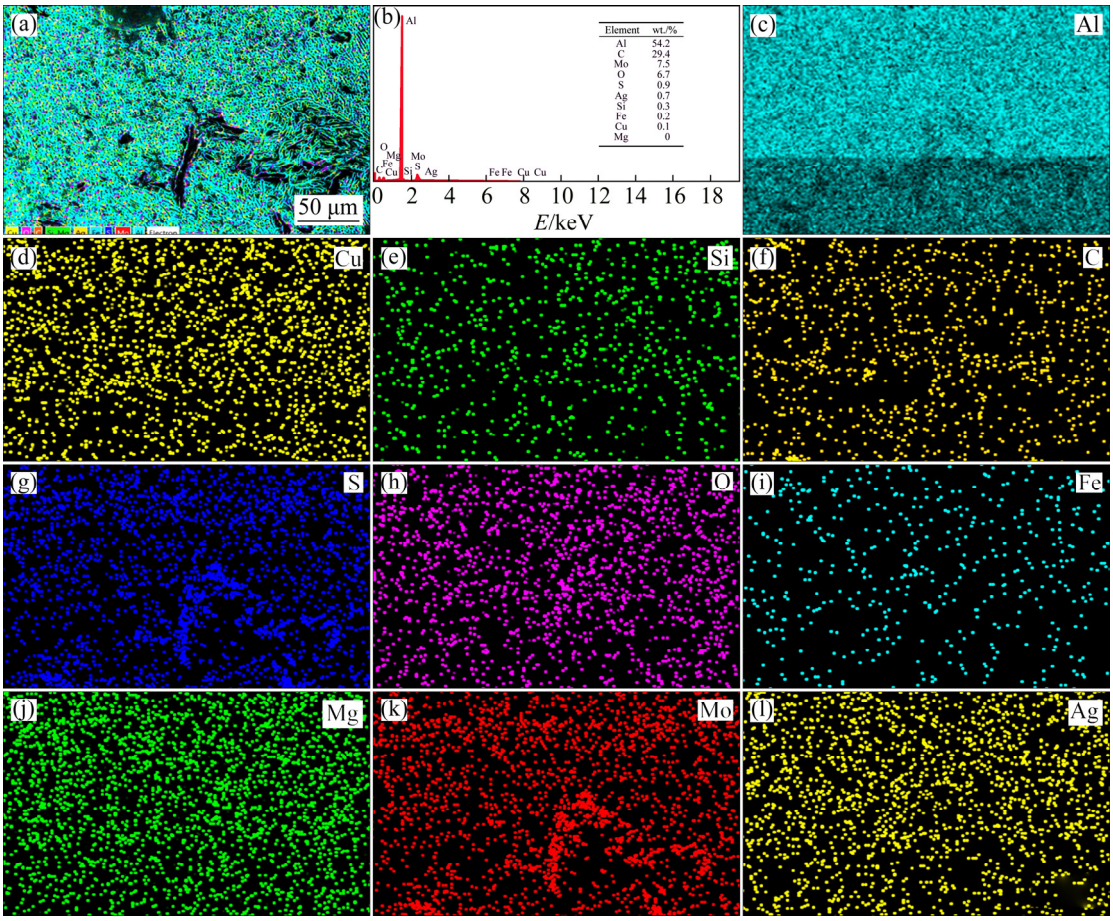

Fig. 15 SEM image (a), EDS spectrum (b) and element mapping images (c−l) of as-cast Al−4.5Cu/10SiC/4MoS_2 composite

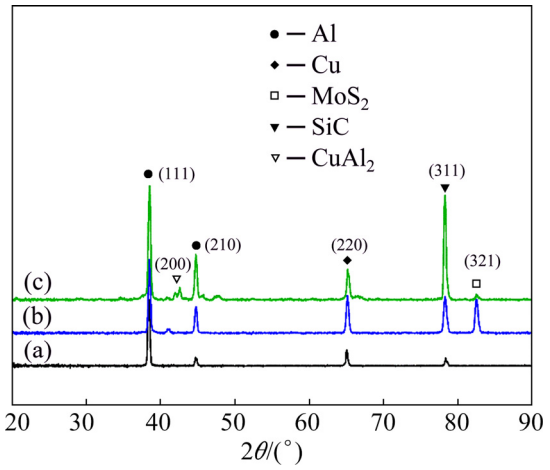

Fig. 16 XRD patterns of LSM-treated matrix and hybrid composites at LSE of 38 J/mm^2: (a) Al−4.5Cu; (b) Al−4.5Cu/10SiC/2MoS_2; (c) Al−4.5Cu/10SiC/4MoS_2

significantly in all the cases. For the matrix after LSM, the highest hardness of $HV_{0.1}$ 102 is observed at LSE of 38 J/mm^2 and the lowest hardness of $HV_{0.1}$ 82 is observed at 45 J/mm^2. For Al−4.5Cu/10SiC/2MoS_2 composite after LSM, the highest hardness of $HV_{0.1}$ 141 was observed at LSE of 38 J/mm^2 and the lowest hardness of $HV_{0.1}$ 99 is observed at 45 J/mm^2. For Al−4.5Cu/10SiC/ 4MoS_2 after LSM, the highest hardness of $HV_{0.1}$ 149 is observed at LSE 38 J/mm^2 and the lowest hardness of $HV_{0.1}$ 128 is observed at 45 J/mm^2.

The enhancement of microhardness after LSM is due to the following mechanisms.

(1) As the surface temperature is below the melting temperature of reinforcement (SiC+MoS_2), hard particles remain in solid phase during the laser melting process. The melting temperatures of reinforcements (2730 °C for SiC and 1185 °C for MoS_2) are significantly higher than the melting temperature of the aluminum alloy (660 °C). The enhancement of hardness of the composite material due to presence of particles in the matrix alloy improves the overall hardness of the composite. The hard-reinforced particles act as load-bearing elements in the composites resulting in load transfer from matrix alloy to hard ceramic particles by the matrix−particle interface [44].

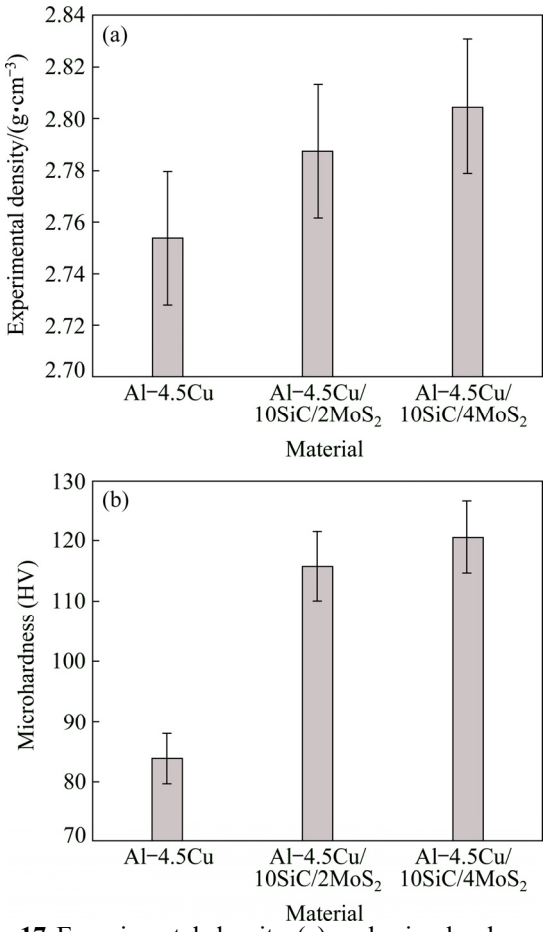

Fig. 17 Experimental density (a) and microhardness (b) of as-cast materials

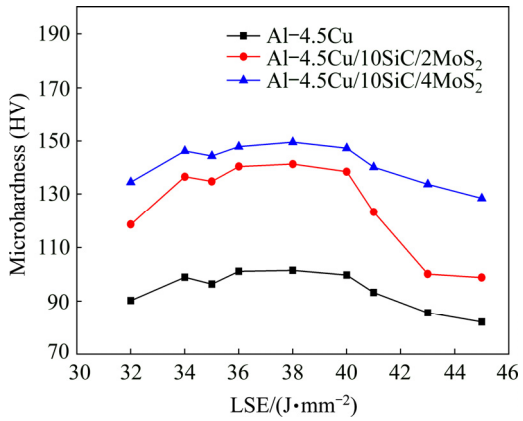

Fig. 18 Effect of LSE on microhardness of LSM-treated material

(2) Thermal expansion coefficients (CTEs) of reinforcement particles and matrix alloy are different. The difference in CTE generates strain fields around reinforcement particles due to rapid solidification process. The movement of dislocations gets obstructed by strain fields when load is applied. The strengthening may take place due to the movement of dislocations getting obstructed or delayed in the composites. Indirect strengthening arises due to high thermal mismatch occurring from irregular cooling among the matrix alloy and ceramic particles. The Al−4.5Cu/BLA fabricated composites may be characterized by a higher difference in CTE of the matrix alloy and the reinforced particles (CTE of Al−4.5Cu alloy is 22.8×10^{-6} °C^{-1}, the CTE of SiC is 4.3×10^{-6} °C^{-1} and the CTE of MoS_2 is 7.4×10^{-6} °C^{-1}). The differences in CTE produce strain fields around particles during the solidification process. The movement of dislocations may be obstructed by strain fields and the larger applied load may be required for moving the dislocations around the strain fields [45−47].

(3) LSM produces fine-grain structure, which in turn enhances the yield stress σ_y of the material as per the following Hall−Petch relation [48]:

$$\sigma_y = \sigma_o + kd^{-1/2} \quad (6)$$

where σ_o is the friction stress, k is the Hall−Petch coefficient, and d is the grain size. The grain size mainly depends on material composition, addition of grain refiner (e.g. reinforcements) and solidification rate. The grain refiners (reinforcement particles) increase the number of heterogeneous nucleating sites [49]. Hall−Petch relationship describes that the strength of the composite is inversely proportional to the square root of grain size. The mean distance of a dislocation travel may be decreased with reducing grain size, which quickly starts heap-up of dislocations at grain boundaries [50]. Grain size is the most significant feature in enhancing the hardness. At a LSE of 38 J/mm^2, the highest microhardness is observed due to the finest grain size. At LSE of 45 J/mm^2, microhardness is the lowest. A high LSE creates deeper melted region of material with coarse grains. PINTO et al [51] also observed the increase in hardness due to LSM of an Al−Cu alloy. GRABOWSKI and MOSKAL [20] fabricated $AlSi_{12}/SiC_p$ composite by stir casting method and carried out LSM; they also observed an enhancement of hardness due to LSM.

3.4 Corrosion resistance in acid and salt solutions

The evaluation of corrosion attack on surface of matrix alloy and composite was carried out after corrosion immersion test in acid solution (2.5%

H_2SO_4) and alkaline (salt) solution (5% NaCl) by mass loss method. The pH values were 0.74 and 9.08 for acid and salt solutions, respectively. The corrosion mass loss values of the as-cast matrix and composites are caused by corrosion damages in acid and salt solutions, as shown in Fig. 19. The mass losses of as-cast material in salt environment are 0.061 g for matrix alloy, 0.048 g for Al−4.5Cu/10SiC/2MoS_2 and 0.041 g for Al−4.5Cu/10SiC/4MoS_2 composites. The as-cast material mass losses in acidic environment are 0.072 g for matrix alloy, 0.064 g for Al−4.5Cu/10SiC/2MoS_2 and 0.057 g for Al−4.5Cu/10SiC/4MoS_2 composites. It is clear from Fig. 19 that corrosion mass loss is more for all materials in acidic environment. Composites have better corrosion resistance than as-cast matrix material. Moreover, with the increase in the mass fraction of MoS_2, the corrosion resistance increases.

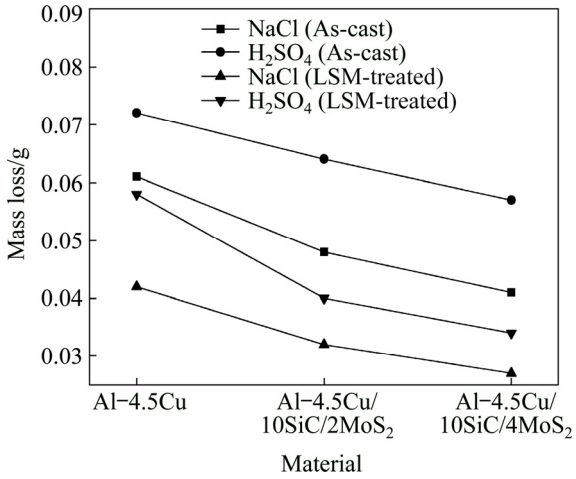

Fig. 19 Mass losses due to corrosion for as-cast and LSM-treated composites

The corrosion mass losses of LSM-treated matrix and composites at LSE of 38 J/mm^2 are also shown in Fig. 19. The material mass losses in salt environment are 0.042 g for matrix alloy, 0.032 g for Al−4.5Cu/10SiC/2MoS_2 and 0.027 g for the Al−4.5Cu/10SiC/4MoS_2 composites. The corresponding values in acidic environment are 0.058 g for matrix alloy, 0.04 g for Al−4.5Cu/10SiC/2MoS_2 and 0.034 g for Al−4.5Cu/10SiC/4MoS_2 composites. Thus, mass loss due to acid corrosion attack is higher than that due to salt corrosion attack. Overall, corrosion resistance is improved after LSM treatment due to elimination of porosity and fine grain structure.

Figures 20−23 show the surface morphologies of as-cast and LSM-treated matrix alloy and composite after acid and alkaline corrosion immersion tests, carried out for 200 h. In the as-cast matrix material, corrosion is in the form of uniformly distributed holes called pits as shown in

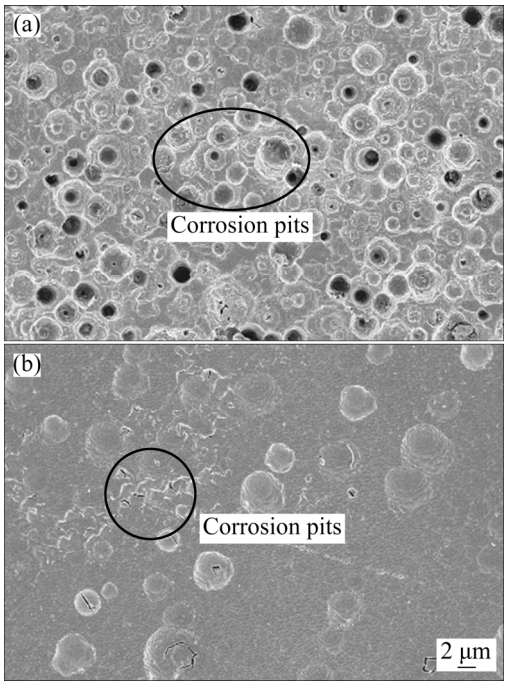

Fig. 20 Surface morphologies of corroded matrix material in 5% NaCl after 200 h corrosion test: (a) As-cast; (b) LSM-treated

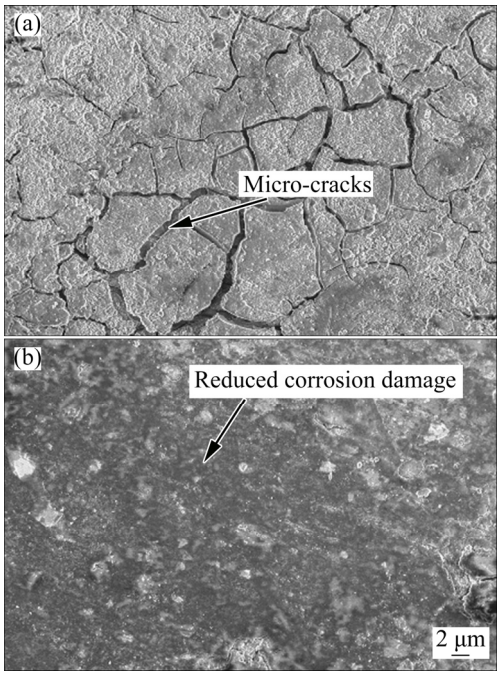

Fig. 21 Surface morphologies of corroded matrix material in 2.5 mol/L H_2SO_4 after 200 h corrosion test: (a) As-cast; (b) LSM-treated

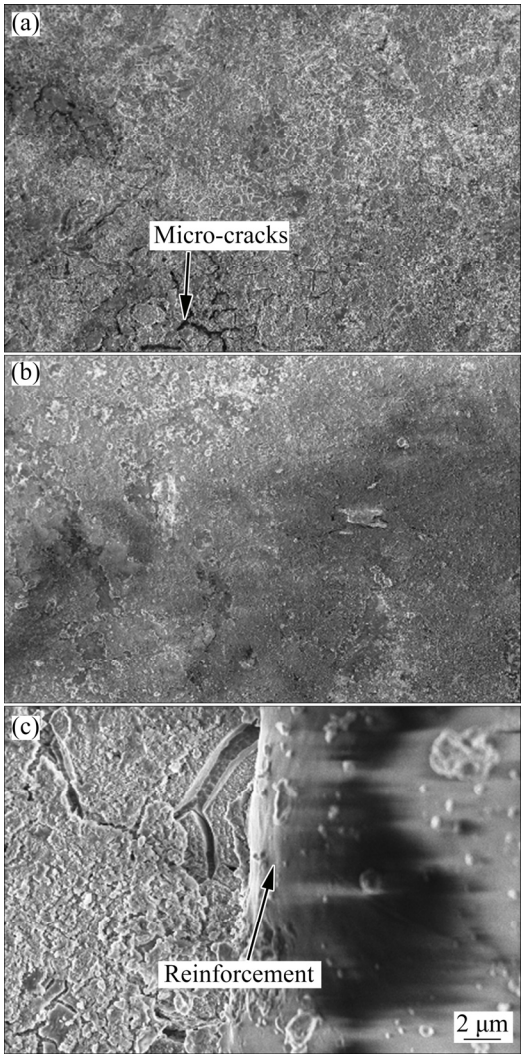

Fig. 22 Surface morphologies of corroded Al−4.5Cu/10SiC/4MoS_2 composite material in 5% NaCl after 200 h corrosion test: (a) As-cast; (b) LSM-treated; (c) Un-corroded reinforcement after LSM

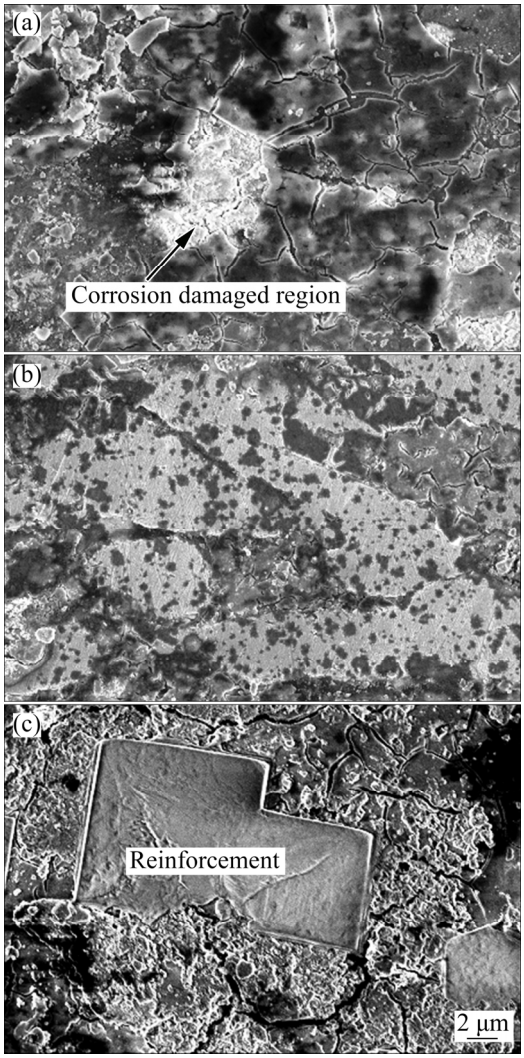

Fig. 23 Surface morphologies of corroded Al−4.5Cu/10SiC/4MoS_2 composite material in 2.5 mol/L H_2SO_4 after 200 h corrosion test: (a) As-cast; (b) LSM-treated; (c) Un-corroded reinforcement after LSM

Fig. 20(a) in salt environment. These are not observed after LSM (Fig. 20(b)). The micro-crakes are observed in acidic environment on the surface of as-cast matrix (Fig. 21(a)); reduction in corrosion damage can be seen on the matrix surface after LSM (Fig. 21(b)). A comparison of Fig. 20(a) and Fig. 21(a) reveals that the layer of corrosion produced is much more uniform in the acidic environment than that in salt; the extent of corrosion is more in the acid.

The corroded surface morphologies of as-cast and LSM-treated Al−4.5Cu/10SiC/4MoS_2 composite after salt corrosion immersion tests are shown in Fig. 22. The corrosion damage is higher in the as-cast composite and micro-cracks appear (Fig. 21(a)); less corrosion damage is observed in the composite after LSM (Fig. 22(b)). Pit size on the as-cast surface of material is significantly larger than that in the LSM-treated composite. In the composite, boundaries of reinforcement particles remain uncorroded (Fig. 22(c)).

The corroded surface morphologies of the as-cast and LSM-treated Al−4.5Cu/10SiC/4MoS_2 composite after acid corrosion immersion test are shown in Fig. 23. The micro-cracks and more corrosion damage regions are observed in the as-cast composite in acidic environment (Fig. 23(a)). After laser treatment only slight corrosion damage is observed along the boundaries in the form of thin cracks (Fig. 23(b)). In the LSM-treated composites,

boundaries of dispersed reinforcement particles remain uncorroded (Fig. 23(c)).

In the acidic solution, the sizes of corrosion pit and micro-cracks are larger; the swelling on the surface of the sample in the acidic solution is due to internal pressure of corroded material. It is confirmed from the results that the corrosion attack is higher in the acidic environment (Figs. 21 and 23) than that in the salt environment (Figs. 20 and 22). LSM improves corrosion resistance. Similarly, YUE et al [52] noticed that the corrosion resistance of AA7075 aluminium alloy after LSM got improved. ZHANG et al [53] observed that corrosion resistance of Al−SiC composites was improved after LSM. The corrosion resistance is higher for the LSM-treated material in salt and acidic environments compared with as-cast material. This is attributed to the redistribution of the second phase (reinforcement) particles on the LSM-treated material. The presence of magnificently dispersed particles and metastable phases leads to the enhancement in corrosion resistance of material after LSM. The dense and homogenous structure forming after LSM protects from corrosion damage. The LSM by 2.5 kW CO_2 laser machine is claimed to be beneficial for aluminium alloys from corrosion point of view and consequently deserves further investigation for the development of novel materials.

3.5 Wear behaviour of as-cast and LSM-treated material

The variation in the wear rate of the as-cast Al−4.5Cu alloy and SiC+MoS_2 reinforced composites is shown in Fig. 24. The wear rate of matrix alloy increases with an increase in applied load as shown in Fig. 24 at sliding speeds of 1.5 and 3.5 m/s. This is due to direct contact of soft matrix alloy with hard disc material.

The wear rate of the matrix alloy significantly decreases by the presence of SiC, which acts as load-bearing element, resulting in the increase in wear resistance of the composite. The presence of MoS_2 produces a protective layer to separate the mating pairs and acts as a solid lubricant, resulting in a notable reduction in the wear rate of the composites [54]. The wear rate of Al−4.5Cu/SiC/MoS_2 composites is less than that of the matrix alloy, which indicates that the wear resistance of the composites increases with the addition of reinforcement content. The hardness of the fabricated composites is also a key point to enhance the wear resistance. The incorporation of SiC particles significantly hardens the material, causing a drastic reduction of the wear rate. Increasing the mass fraction of MoS_2 from 2% to 4% does not have a significant influence on the wear rate. A comparison of Fig. 24(a) with Fig. 24(b) shows that the wear rate is slightly reduced with the increase in sliding speed. Although the heat generation due to friction is more at higher sliding speed, less time is available for covering a specified distance. Hence, the overall effect is slightly reduced in the wear rate.

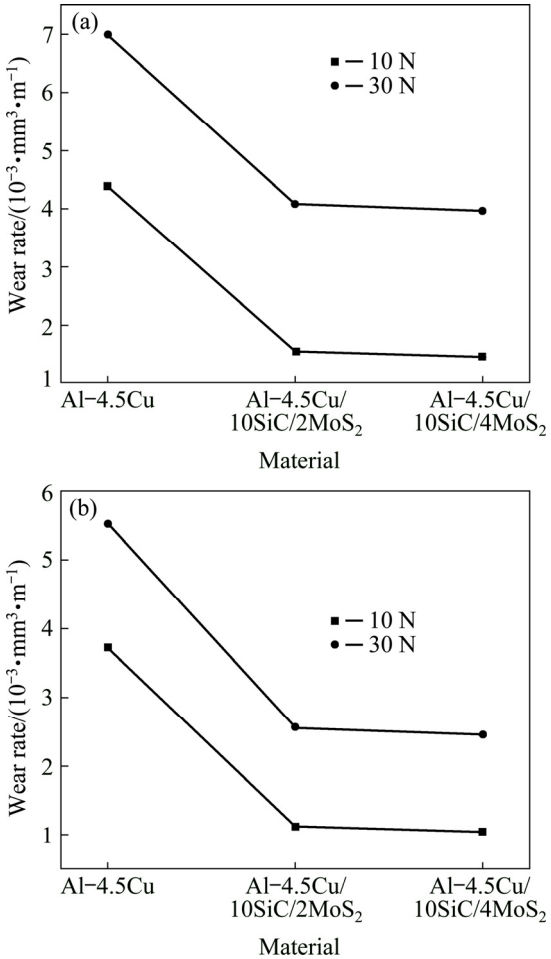

Fig. 24 Wear rates of as-cast material at different sliding speeds: (a) 1.5 m/s; (b) 3.5 m/s

Further improvement of wear resistance of the matrix and composite material is achieved with secondary operation for surface development treatment, i.e. after LSM. The laser treatment of matrix alloy and its composites has a significant effect on the wear behaviour of matrix alloy and its composites, as shown in Fig. 25. For applied load

of 10 N and sliding speed of 1.5 m/s, a 30% reduction in wear rate is observed when compared with as-cast matrix alloy, as shown in Fig. 25(a). Reductions of 32% and 38% are observed in the wear rate after LSM for hybrid composites having 2% and 4% of MoS_2, respectively, as shown in Fig. 25(a). At applied load of 30 N and sliding speed of 3.5 m/s, LSM reduces the wear rate by 29%, 35% and 33% for as-cast matrix alloy and hybrid composites having 2% and 4% of MoS_2, respectively, as shown in Fig. 25(b). The improvement in wear resistance after LSM is due to the grain refinement of surface, uniform distribution of reinforcement particles and reduction in porosity apart from the enhancement of hardness. The maximum wear resistance is attained after LSM for Al−4.5Cu/10SiC/4MoS_2 at an applied load of 10 N and a sliding speed of 3.5 m/s. The protective covering generated by solid lubricant MoS_2 also contributes to wear resistance of composites. STAIA et al [55] fabricated A-356 aluminium alloy/WC composite by a laser alloying technique.

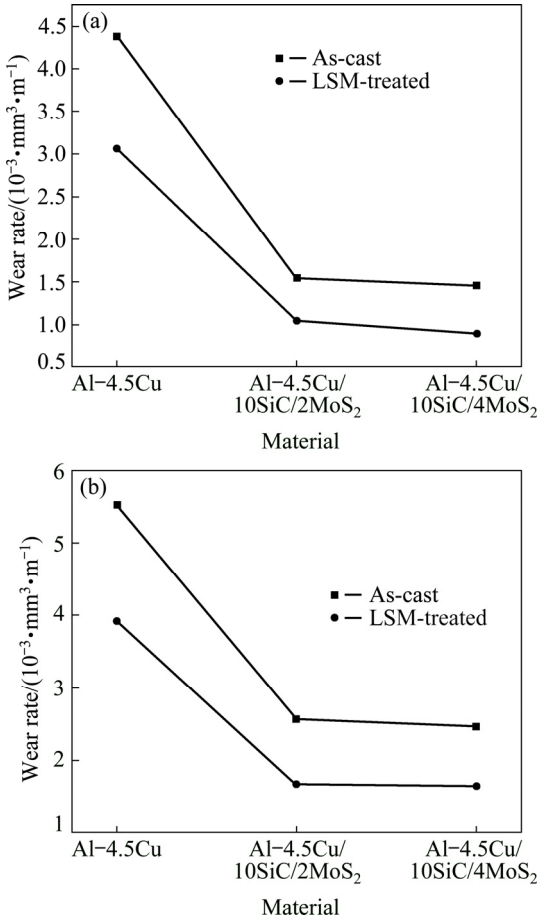

Fig. 25 Wear rates of composite material before and after LSM under different conditions: (a) 1.5 m/s, 10 N; (b) 3.5 m/s, 30 N

It was reported that smaller wear resistance depends on the processing parameters. HUANG et al [56] have reported that the surface of pure aluminum and AA7075 aluminum alloy provided better wear resistance by Al_2O_3 ceramic coating by laser. ROUHI et al [57] studied the effect of SiC and MoS_2 on wear behavior of Al matrix composites.

The dry sliding wear mechanism of Al−4.5Cu/SiC/MoS_2 hybrid composites before and after LSM (at LSE of 38 J/mm^2) was investigated to identify the effect of load, sliding speed and reinforcement particles. Delamination is observed in the matrix but not in the composite. Ridges and deep grooves occur due to hard asperities of counter steel disc. Ploughing, i.e. cutting the surface of test pin, leads to wear by the removal of small fragments of materials. Delaminated plastic deformation areas are also observed at a higher load of 30 N on surface of matrix alloy. This is not observed in the reinforced composite. For the sake of brevity, micrographs after wear are not shown in this work.

4 Conclusions

(1) In Al−4.5Cu and Al−4.5Cu/SiC/MoS_2 composite materials, LSM refined the micro-structure and eliminated porosity by forming a homogeneous melted layer. The grain size was very small at LSE of 38 J/mm^2 for all the materials. At a higher LSE of 45 J/mm^2, the agglomeration of particles and cracked particles was observed in the Al−4.5Cu/10SiC/4MoS_2 composite; micro-pores were close to the agglomerated reinforcement particles.

(2) The LSM enhanced the hardness. The highest hardness was noticed in the Al−4.5Cu/10SiC/4MoS_2 composite after LSM at LSE of 38 J/mm^2.

(3) The corrosion behaviour of as-cast and LSM-treated materials was observed in acidic and alkaline (salt) environments by mass loss method. The acidic environment produced more corrosion damage than the salt environment. LSM improved the corrosion resistance. The highest mass loss was 0.072 g in the as-cast matrix in the acidic solution and the lowest mass loss was 0.027 g in the LSM-treated Al−4.5Cu/10SiC/4MoS_2 composite in the salt solution.

(4) The wear rate of as-cast composite decreased with the addition of hard ceramic SiC

particles and solid lubricant MoS_2 into the matrix alloy. Furthermore, the improvement in wear resistance occurred after LSM. The highest wear resistance was observed in the LSM-treated hybrid composites of Al−4.5Cu/10SiC/4MoS_2 at LSE of 38 J/mm^2. However, reducing the mass fraction of MoS_2 did not cause significant change in wear-behaviour.

Acknowledgments

Authors acknowledge the DST-FIST scheme of India that enables to procure CO_2 laser facility. They also thank Indian Institute of Technology Guwahati for inducting the first author, Dr. Praveen Kumar BANNARAVURI, as a full time post-doctoral fellow.

References

[1] HEINZ A, HASZLER A, KEIDE C, MOLDENHAUER S, BENEDICTUS R, MILLER W S. Recent development in aluminium alloys for aerospace applications [J]. Materials Science and Engineering A, 2000, 280: 102−107.

[2] ABBASIPOUR B, NIROUMAND B, VAGHEFI S M M, ABEDI M. Tribological behavior of A356−CNT nanocomposites fabricated by various casting techniques [J]. Transactions of Nonferrous Metals Society of China, 2019, 29: 1993−2004.

[3] PRABHU S R, SHETTIGAR A K, HERBERT M A, RAO S S. Microstructure and mechanical properties of rutile-reinforced AA6061 matrix composites produced via stir casting process [J]. Transactions of Nonferrous Metals Society of China, 2019, 29: 2229−2236.

[4] BANNARAVURI P K, BIRRU A K. Strengthening of mechanical and tribological properties of Al−4.5%Cu matrix alloy with the addition of bamboo leaf ash [J]. Results in Physics, 2018, 10: 360−373.

[5] FAN Cai-he, OU Ling, HU Ze-yi, YANG Jian-jun, CHEN Gang, YAN Hong-ge. Microstructures and mechanical properties of BP/7A04 Al matrix composites [J]. Transactions of Nonferrous Metals Society of China, 2019, 29: 2027−2034.

[6] KUMAR B P, BIRRU A K. Microstructure and mechanical properties of aluminium metal matrix composites with addition of bamboo leaf ash by stir casting method [J]. Transactions of Nonferrous Metals Society of China, 2017, 27: 2555−2572.

[7] PAN L, HAN J, YANG Z, LI X, WANG J, LI Z, LI W. Thermal fatigue crack behavior of SiCp/A356 composites prepared by stirring casting [J]. Results in Physics, 2017, 7: 927−933.

[8] PUGALENTHI P, JAYARAMAN M, SUBBURAM V. Study of the microstructures and mechanical properties of aluminium hybrid composites with SiC and Al_2O_3 [J]. Materials and Technology, 2019, 53: 49−55.

[9] SINGH G, GOYAL S. Microstructure and mechanical behavior of AA6082-T6/SiC/B4C-based aluminum hybrid composites [J]. Particulate Science and Technology, 2018, 36: 154−161.

[10] SINGH S, SINGH R, SINGH G S. Investigations for surface hardness of aluminum matrix composites with hybrid reinforcement [J]. Transactions of the Indian Institute of Metals, 2019, 72: 181−190.

[11] JOJITH R, RADHIKA N. Mechanical and tribological properties of LM13/TiO_2/MoS_2 hybrid metal matrix composite synthesized by stir casting [J]. Particulate Science and Technology, 2018, 37: 570−582.

[12] CHEN R, ZHANG G. Casting defects and properties of cast A356 aluminium alloy reinforced with SiC particles [J]. Composites Science and Technology, 1993, 47: 51−56.

[13] SHARMA S C, RAMESH A. Effect of heat treatment on mechanical properties of particulate reinforced Al6061 composites [J]. Journal of Materials Engineering and Performance, 2000, 9: 557−561.

[14] ROHATGI P K, YARANDI F M, LIU Y, ASTHANA R. Segregation of silicon carbide by settling and particle pushing in cast aluminum−silicon−carbide particle composite [J]. Materials Science and Engineering A, 1991, 147: L1−L6.

[15] JIRU W G, SANKAR M R, DIXIT U S, LIAO H. Laser surface melting of Al−12Si−4Cu−1.2Mn alloy [J]. International Journal of Mechatronics and Manufacturing Systems, 2018, 11: 230−249.

[16] JIRU W G, SANKAR M R, DIXIT U S. Laser surface alloying of copper, manganese, and magnesium with pure aluminum substrate [J]. Journal of Materials Engineering and Performance, 2016, 25: 1172−1181.

[17] IWATANI S, OGATA Y, UENISHI K, KOBAYASHI K F, TSUBOI A. Laser cladding of Fe−Cr−C alloys on A5052 aluminum alloy using diode laser [J]. Materials Transactions, 2005, 64: 1341−1347.

[18] YUE T M, YAN L J, CHAN C P, DONG C F, MAN H C, PANG G K H. Excimer laser surface treatment of aluminium alloy AA7075 to improve corrosion resistance [J]. Surface and Coatings Technology, 2004, 179: 158−164.

[19] RAMS J, PADRO A, URENA A, ARRABAL R, VIEJO F, LOPEZ A J. Surface treatment of aluminium matrix composites using a high power diod laser [J]. Surface and Coatings Technology, 2007, 202: 1199−1203.

[20] GRABOWSKI A, MOSKAL G. Laser surface treatment of aluminium matrix composites [C]//Applications of Lasers, Proceedings of SPIE. Szczecin, Poland: Society of Photo-Optical Instrumentation Engineers (SPIE), 2012. DOI: 10.1117/12.2013588.

[21] PARIONA M M, TELEGINSKI V, dos SANTOS K, de LIMA A A, ZARA A J, MICENE K T, RIVA R. Influence of laser surface treated on the characterization and corrosion behavior of Al−Fe aerospace alloys [J]. Applied Surface Science, 2013, 276: 76−85.

[22] QUAZI M M, FAZAL M A, HASEEB A S M A, YUSOF F, MASJUKI H H, ARSLAN A. Laser-based surface modifications of aluminum and its alloys [J]. Critical Reviews in Solid State and Materials Sciences, 2016, 41:

106−131.

[23] OSORIO W R, CHEUNG N, PEIXOTO L C, GARCIA A. Corrosion resistance and mechanical properties of an Al−9wt.%Si alloy treated by laser surface remelting [J]. International Journal of Electrochemical Science, 2009, 4: 820−831.

[24] WONG T T, LIANG G Y. Effect of laser melting treatment on the structure and corrosion behaviour of aluminium and Al−Si alloys [J]. Journal of Materials Processing Technology, 1997, 63: 930−934.

[25] OSORIO W R, CHEUNG N, SPINELLI J E, CRUZ K S, GACIA A. Microstructural modification by laser surface remelting and its effect on the corrosion resistance of an Al−9wt.%Si casting alloy [J]. Applied Surface Science, 2008, 254: 2763−2770.

[26] HU J, KONG L C, LIU G. Structure and hardness of surface of $Al_{18}B_4O_{33w}$/Al composite by laser surface melting [J]. Materials Science and Engineering A, 2008, 486: 80−84.

[27] QIAN D. Microstructure and corrosion performance of excimer laser-melted AA2124-T4 aluminium alloy and SiC_p/AA2124-T4 composite [D]. Manchester: School of Materials, Corrosion and Protection Centre, University of Manchester, 2015.

[28] YILBAS B S, KARATAS C, KARAKOC H, ALEEM B A, KHAN S, AL-AQEELI N. Laser surface treatment of aluminum based composite mixed with B_4C particles [J]. Optics and Laser Technology, 2015, 66: 129−137.

[29] JUANG S H, FAN L J, YANG H P O. Influence of preheating temperatures and adding rates on distributions of fly ash in aluminum matrix composites prepared by stir casting [J]. International Journal of Precision Engineering and Manufacturing, 2015, 16: 1321−1327.

[30] BHUYAN M, KANT R, JOSHI S N. Experimental investigation on laser bending of metal sheets using parabolic irradiations [C]//Proceedings of the 5th International & the 26th All India Manufacturing Technology, Design and Research Conference (AIMTDR 2014). IIT Guwahati, Assam, India, 2014: 708-1.

[31] ARDILA-RODRIGUEZ L A, MENEZES B R C, PEREIRA L A, TAKAHASHI R J, OLIVEIRA A C, TRAVESSA D N. Surface modification of aluminum alloys with carbon nanotubes by laser surface melting [J]. Surface & Coatings Technology, 2019, 377: 124930. DOI: 10.1016/j.surfcoat. 2019.124930.

[32] SUN H. Thin lens equation for a real laser beam with weak lens aperture truncation [J]. Optical Engineering, 1998, 37: 2906−2914.

[33] KANT R, JOSHI S N, DIXIT U S. An integrated FEM−ANN model for laser bending process with inverse estimation of absorptivity [J]. Mechanics of Advanced Materials and Modern Processes, 2015, 1: 1−12.

[34] KADHIM M J, AL-RUBAIEY S I, HAMMOOD A S. The influence of laser specific energy on laser sealing of plasma sprayed yttria partially stabilized zirconia coating [J]. Optics and Lasers in Engineering, 2013, 51: 159−166.

[35] GUPTA M, LAI M O, SOO C Y. Effect of type of processing on the microstructural features and mechanical properties of Al−Cu/SiC metal matrix composites [J]. Materials Science and Engineering A, 1996, 210: 114−122.

[36] GUI M C, HAN J M, LI P Y. Microstructure and mechanical properties of Mg−Al_9Zn/SiC_p composite produced by vacuum stir casting process [J]. Materials Science and Technology, 2004, 20: 765−771.

[37] NAYAK S. Laser induced surface modification of aluminium alloys [D]. Knoxville: The University of Tennessee, 2004.

[38] DAS D K, MISHRA P C, SINGH S, THAKUR R K. Properties of ceramic-reinforced aluminium matrix composites — A review [J]. International Journal of Mechanical and Materials Engineering, 2014, 9(1): Article 16, 1−16.

[39] KOGAN Y D, SAZONOVA Z S, ALEKSANDROV V D, BOROVSKAYa T M. Antifriction properties of aluminum alloys after surface laser alloying [J]. Metal Science and Heat Treatment, 1991, 33: 772−776.

[40] MCCAFFERTY E, SHAFRIN E G, MCKAY J A. Microstructural and surface modification of an aluminum alloy by rapid solidification with a pulsed laser [J]. Surface Technology, 1981, 14: 219−223.

[41] DAS S, YEGNESWARAN A H, ROHATGI P K. Characterization of rapidly solidified aluminium−silicon alloy [J]. Journal of Materials Science, 1987, 22: 3173−3177.

[42] HUANG W C, CHUANG C S, LIN C C, WU C H, LIN D Y, LIU S H, TSENG W P, HORNG J B. Microstructure-controllable laser additive manufacturing process for metal products [J]. Physics Procedia, 2014, 56: 58−63.

[43] SUREKHA K, MURTY B S, RAO K P. Comparison of corrosion behaviour of friction stir processed and laser melted AA 2219 aluminium alloy [J]. Materials and Design, 2011, 32: 4502−4508.

[44] MILAN M T, BOWEN P. Tensile and fracture toughness properties of SiC_p reinforced Al alloys: Effects of particle size, particle volume fraction and matrix strength [J]. Journal of Materials Engineering and Performance, 2004, 13: 775−783.

[45] ZHANG J, PEREZ R J, LAVERNIA E J. Dislocation-induced damping in metal matrix composites [J]. Journal of Materials Science, 1993, 28: 835−846.

[46] VOGT R, ZHANG Z, LI Y, BONDS M, BROWNING N D, LAVERNIA E J, SCHOENUNG J M. The absence of thermal expansion mismatch strengthening in nanostructured metal-matrix composites [J]. Scripta Materialia, 2009, 61: 1052−1055.

[47] KURUVILLA A K, BHANUPRASAD V V, PRASAD K S, MAHAJAN Y R. Effect of different reinforcements on composite-strengthening in aluminium [J]. Bulletin of Materials Science, 1989, 12: 495−505.

[48] WYRZYKOWSKI J W, GRABSKI M W. The Hall−Petch relation in aluminium and its dependence on the grain boundary structure [J]. Philosophical Magazine A, 1986, 53: 505−520.

[49] DHANASEKARAN S, SUNILRAJ S, RAMYA G, RAVISHANKAR S. SiC and Al_2O_3 Reinforced aluminum metal matrix composites for heavy vehicle clutch applications [J]. Transactions of the Indian Institute of Metals, 2016, 69: 699−703.

[50] BANNARAVURI P K, BIRRU A K. Strengthening of mechanical and tribological properties of Al−4.5%Cu matrix alloy with the addition of bamboo leaf ash [J]. Results in

Physics, 2018, 10: 360−373.
[51] PINTO A M, CHEUNG N, IERARDI M C F, GARCIA A. Microstructural and hardness investigation of an aluminium−copper alloy processed by laser surface melting [J]. Materials Characterization, 2003, 50: 249−253.
[52] YUE T M, YAN L J, CHAN C P. Stress corrosion cracking behavior of Nd :YAG laser-treated aluminum alloy 7075 [J]. Applied Surface Science, 2006, 252: 5026−5034.
[53] ZHANG X M, MAN H C, YUE T M. Corrosion properties of excimer laser surface treated Al−SiC metal matrix composite [J]. Scripta Materialia, 1996, 35: 1095−1100.
[54] DANIEL A A, MURUGESAN S, KUMAR M, SUKKASAMY S. Dry sliding wear behaviour of aluminium 5059/SiC/MoS_2 hybrid metal matrix composites [J]. Materials Research, 2017, 20(6): 1697−1706.
[55] STAIA M H, CRUZ M, DAHOTRE N B. Wear resistance of a laser alloyed A-356 aluminum/WC composite [J]. Wear, 2001, 251: 1459−1468.
[56] HUANG K, LIN X, CHANGSHENG X I E, YUE T M. Microstructure and wear behaviour of laser-induced thermite reaction Al_2O_3 ceramic coatings on pure aluminum and AA7075 aluminum alloy [J]. Journal of Wuhan University of Technology, 2008, 23(1): 89−94. DOI 10.1007/s11595-006-1089-7.
[57] ROUHI M, MOAZAMI-GOUDARZI M, ARDESTANI M. Comparison of effect of SiC and MoS_2 on wear behavior of Al matrix composites [J]. Transactions of Nonferrous Metals Society of China, 2019, 29: 1169−1183.

激光表面熔化对 SiC 和 MoS_2 颗粒增强 Al−4.5Cu 复合材料表面完整性的影响

Praveen Kumar BANNARAVURI[1], Anil Kumar BIRRU[2], Uday Shanker DIXIT[3]

1. Department of Mechanical Engineering, Karunya Institute of Technology and Science, Coimbatore, Tamil Nadu 641114, India;
2. Department of Mechanical Engineering, National Institute of Technology Manipur, Imphal 795004, India;
3. Department of Mechanical Engineering, Indian Institute of Technology Guwahati, Assam 781039, India

摘　要：以 Al−4.5Cu 合金为基体，用搅拌铸造法制备两种复合材料。一种是用 10% SiC(质量分数)和 2% MoS_2(质量分数)进行增强，另一种是用 10% SiC(质量分数)和 4% MoS_2(质量分数)进行增强。为了研究激光表面熔化(LSM)对材料表面性能的影响，采用 CO_2 激光束对材料表面进行重熔。研究激光熔化表面的形貌、显微硬度、耐蚀性和耐磨性。将 LSM 后的整体表面完整性与铸态表面进行比较。结果表明，LSM 能提高每种情况下表面的显微硬度和耐磨性。激光熔化表面孔隙率低，耐蚀性高。因此，LSM 可以方便地应用于提高铝基复合材料的表面完整性。然而，在本研究中存在一个最佳的激光比能以获得最佳的表面完整性，约为 38 J/m^2。

关键词：铝基复合材料；碳化硅；二硫化钼；激光表面熔化；显微硬度；耐腐蚀性

(Edited by Wei-ping CHEN)